**International Journal for Numerical Methods in Engineering, Volume 121, Issue 8, Apr 2020**

**DOI**: https://doi.org/10.1002/nme.6282

Received: 00 Month 0000 | Revised: 00 Month 0000 | Accepted: 00 Month 0000

DOI: xxx/xxxx

RESEARCH ARTICLE

# Large-Step Explicit Time Integration via Mass Matrix Tailoring

José A. González[1] | K. C. Park[2]

[1]Escuela Técnica Superior de Ingeniería, Universidad de Sevilla, Camino de los Descubrimientos s/n, Seville E-41092, Spain

[2]Ann and H. J. Smead Aerospace Engineering Sciences, University of Colorado, Boulder, CO 80309-429, USA

**Correspondence**
K. C. Park, University of Colorado, Boulder, CO 80309-429, USA. Email: kcpark@colorado.edu

**Abstract**

A method for tailoring mass matrices that allows large time step explicit transient analysis is presented. It is shown that the accuracy of the present tailored mass matrix preserves the low-frequency contents while effectively replacing the unwanted higher mesh frequencies by a user-desired cut-off frequency. The proposed mass tailoring methods are applicable to elemental, substructural as well as global systems, requiring no modifications of finite element generation routines. It becomes most computationally attractive when used in conjunction with partitioned formulation as the number of higher (or lower) modes to be filtered out (or retained) are significantly reduced. Numerical experiments with the proposed method demonstrate that they are effective in filtering out higher modes in bars, beams, plain stress and plate bending problems while preserving the dominant low-frequency contents.

**KEYWORDS:**
mass matrix tailoring; explicit time integration; partitioned analysis

## 1 | INTRODUCTION

Explicit transient analysis of linear and nonlinear mechanics problems has remained popular, due to simplicity when employing diagonal mass matrices and to some degree as it can accommodate variable time step strategies. It has been recognized that the Courant step size restriction[1] is largely due to the so-called mesh frequencies rather then physical contents when the dynamic response is dominated by low-frequency modes. It should be mentioned that an important exception occurs when the responses are dominated by the propagation of discontinuous stress waves where dispersion accuracy improvements are desired[2,3,4,5,6]. In order to alleviate the step size limitations imposed by the mesh frequencies whose response components contribute very little when low modes dominate the transient responses, various mass matrix tailoring have been introduced by altering the mass matrices in order to reduce/ filter out the high frequencies of the dynamical system without affecting the low-mid frequencies[7,8,9,10,11,12,13,14,15,16,17,18,19,20,21,22,23]. Most of existing methods cited above require either replacing existing elements by tailored elements and/or adopt element component-dependent time stepping procedures, leading to either elemental and/or global approaches, depending on how the modification of the mass matrix is made.

There is another issue which is typically paid only with lip-service attention: software modularity and implementation requirements. Most elemental modification approaches need to modify element mass and/or stiffness generation routines. Perhaps the *spectral scaling* and *global polynomial matrix selective mass scaling*[16] may be viewed as mass scaling methods that require no elemental routine modifications. To the best of our knowledge, the global mass matrix modifications proposed therein leads to dense mass matrix whereas the local mass scaling distorts the original mode shapes. The *multiscale mass scaling*[17] may be classified as a local/global method, in which low frequency response components are approximated by a set of reduced-order bases via *proper orthogonal decomposition* (POD). The mass matrix corresponding to the residual high frequency components are

scaled not in the modal basis but in the physical degrees of freedom contents. Hence, the accuracy of some of the intermediate modes may have been compromised as reported in their numerical experiments.

The preceding review of existing literature indicates that existing mass scaling methods fall into two categories: elemental or global mass matrix modifications. While global approaches can reduce the maximum frequencies of the assembled global system for large-scale models, spectral analysis at the global level becomes computationally infeasible. As for elemental modification approaches, although conceptually simple and easy to implement, it has been shown that the elemental approaches applied at the local level can severely affect accuracy.

In the present work, we propose a *mass matrix tailoring* approach aimed at filtering out the high-frequency response components that are considered *mesh frequencies* or that contribute very little to overall response components, and that can be applied via lower or higher mode shape projection. Specifically, we invoke the following requirements:

1. We rely on existing FEM software requiring no element-level modifications.
2. We avoid modifications in global-level matrix.
3. Most important of all, we employ mass tailoring on substructural level, thus avoiding costly global modifications.
4. To facilitate the preceding requirements, we carry out mass matrix tailoring within the context of *partitioned analysis*[24,25]. One immediate benefit of employing partitioned analysis is its natural adaptation to treat substructural heterogeneities.

Section 2 introduces a simple example of elemental mass tailoring, illustrating the limitations of elemental mass tailoring, even though it preserves the translational mass conservation. From this simple example, specific desirable mass tailoring properties are identified and listed. Section 3 introduces partitioned explicit time marching procedure where the key computational need is the calculation of accelerations for each step marching. Two mass tailoring methods are presented in Sections 4 and 5. The first one is to utilize substructural high-frequency mode shapes together with the cut-off frequency such that all the higher modes are annihilated and replaced by the same cut-off frequency while still preserving the mode-frequency contents for subsequent partitioned analysis. The second is to utilize low-frequency mode shapes which effectively yields the same characteristics except the resulting mass tailoring strategy is different from the first one. In Section 6 it is justified the definition of a cut-off frequency at the substructure level.

Section 7 illustrates the performance of the proposed two mass tailoring methods and show the effectiveness of the present mass tailoring methods via eigenvalue analysis using the scaled mass matrices as compared with the unscaled mass matrices, as applied to vibration analysis of bar, plain stress problem and plate bending vibration problems. The numerical results indicate that one can effectively increase maximum explicit time steps ranging from 4 to 10. Section 8 summarizes the objectives set out in Section 2 and observations accrued from the present study and identifies further studies to make the proposed mass tailoring methods as applied to nonlinear transient analysis.

## 2 | MOTIVATION FOR PRESENT STUDY AND DESIRABLE MASS TAILORING PROPERTIES

This section illustrates a simplest example revealing the limiting features of elemental mass matrix tailoring and sets up requirements for desirable mass matrix tailoring.

### 2.1 | A bar elemental mass tailoring example

Consider an elastic and homogeneous one-dimensional bar discretized with a regular mesh of $N_e$ linear finite elements. The semi-discrete equation of motion of this problem can be written:

$$\mathbf{M}\ddot{\mathbf{u}} + \mathbf{K}\mathbf{u} = \mathbf{f} \tag{1}$$

where the global mass and stiffness matrices are formed by an element by element assembly of finite element contributions given by the expressions:

$$\mathbf{M}_e = \frac{\rho A h_e}{2}\begin{bmatrix}1 & 0\\ 0 & 1\end{bmatrix}, \quad \mathbf{K}_e = \frac{EA}{h_e}\begin{bmatrix}1 & -1\\ -1 & 1\end{bmatrix}, \quad e = 1, 2 \dots N_e \tag{2}$$

**TABLE 1** Maximum global frequency $\omega^{\alpha}_{max}$ for different values of the tailoring parameter $\alpha$ for the FEM bar example with $N_e = 40$ elements and maximum frequency $\omega^{\alpha=0}_{max}$ of Figure 1. The last two columns represent the maximum global frequency scaling and the stepsize gain factor, respectively.

| **Parameter** $\alpha$ | $\omega^{\alpha=0}_{max}$ | $\omega^{\alpha}_{max}$ | $\omega^{\alpha}_{max}/\omega^{\alpha=0}_{max}$ | $\mathsf{N}_{\mathsf{gain}}$ |
|---|---|---|---|---|
| 0 | $\sqrt{2}$ | $\sqrt{2}$ | 1 | 1 |
| 3 | $\sqrt{2}$ | $\frac{1}{\sqrt{2}}$ | $\frac{1}{2}$ | 2 |
| 15 | $\sqrt{2}$ | $\frac{1}{2\sqrt{2}}$ | $\frac{1}{4}$ | 4 |
| 99 | $\sqrt{2}$ | $\frac{1}{\sqrt{50}}$ | $\frac{1}{10}$ | 10 |

with Young's modulus $E$, mass density $\rho$ and element size $h_e$. Eigenvalue analysis of these finite element matrices, reveal that the element presents only one deformational mode shape, given by the mass-normalized eigenvector:

$$\boldsymbol{\Phi}_h = \frac{1}{\sqrt{\rho A h_e}} \begin{bmatrix} 1 \\ -1 \end{bmatrix} \tag{3}$$

associated to the frequency $\omega_e = 2c/h_e$, where $c = \sqrt{E/\rho}$ is the phase velocity of the elastic medium.

Historically, there have been two approaches to tame the mesh frequencies so that one could use a larger explicit integration step, namely, *elemental* mass tailoring and *global* mass tailoring. Elemental mass tailoring can be accomplished with the following transformation of the element mass matrix:

$$\hat{\mathbf{M}}_e = \mathbf{M}_e + \mathbf{M}_e \boldsymbol{\phi}_h \left(\alpha \mathbf{I}_1\right) \boldsymbol{\phi}_h^{\mathsf{T}} \mathbf{M}_e \tag{4}$$

where $\boldsymbol{\phi}_h$ is the elemental mesh mode shape (3), also highest elemental frequency eigenvector for this example and $\alpha > 0$ is a scaling parameter. Note that this tailored mass matrix will be symmetric and positive definite by construction for positive values of $\alpha$. Evaluating the expression for our case, it is obtained:

$$\hat{\mathbf{M}}_e = \frac{\rho A h_e}{2} \begin{bmatrix} 1 + \frac{1}{2}\alpha & -\frac{1}{2}\alpha \\ -\frac{1}{2}\alpha & 1 + \frac{1}{2}\alpha \end{bmatrix} \tag{5}$$

a modified element mass matrix that scales the frequency of the deformational mode by a factor $(1+\alpha)^{-\frac{1}{2}}$.

As an example, let us investigate how global mesh frequencies are affected by the proposed tailored mass matrix (5) considering a bar discretized with $N_e = 40$ finite elements of frequency $\omega_e = \sqrt{2}$. Table 1 presents the global maximum frequency $\omega^{\alpha}_{max}$ obtained for different values of the scaling parameter $\alpha$ and the reduction $\omega^{\alpha}_{max}/\omega^{\alpha=0}_{max} = (1+\alpha)^{-\frac{1}{2}}$ with respect to the unscaled maximum frequency $\omega^{\alpha=0}_{max}$. Because the maximum stable explicit stepsize can be evaluated as $\Delta t^{\alpha} = 2/\omega^{\alpha}_{max}$, the final stepsize gain factor is computed as $\mathsf{N}_{\mathsf{gain}} = \Delta t^{\alpha}/\Delta t^{\alpha=0} = (1+\alpha)^{\frac{1}{2}}$. In Figure 1 we compare the numerical frequencies of the bar with the analytical solution, for different values of the scaling parameter. It is clearly observed how accuracy in the lower modes quickly degrades with the element scaling parameter $\alpha$.

The preceding simple example illustrates that an element-by-element mass tailoring to increase critical time step for explicit transient analysis is not feasible for stepsize increases beyond a factor of 2, at least for the cases of one-dimensional problems.

## 2.2 | Desirable mass tailoring properties

All was not futile with the one-dimensional elemental mass tailoring reported in the preceding demonstration example, though. It demonstrates that the high-frequency filtering scheme given by (4) preserves the low-frequency mode and its mode shape (3) for the bar, the rigid-body mode (associated to $\omega_\alpha = 0$) and its mode shape. In addition, it conserves the total mass of the assembled system.

We are now in a position to stipulate the desirable properties of mass matrix tailoring:

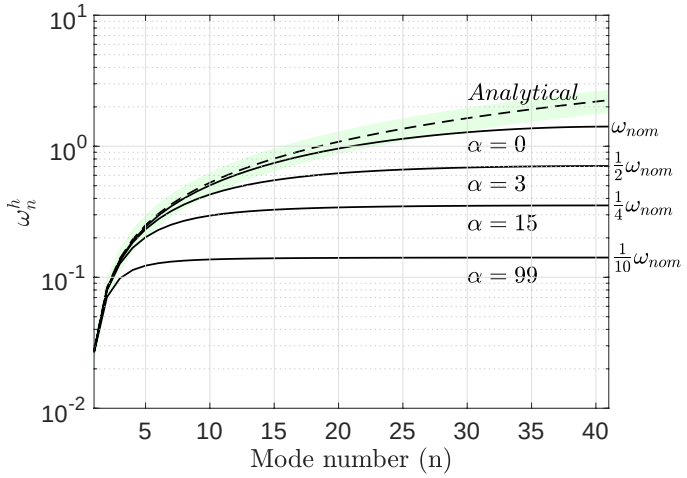


**FIGURE 1** FEM bar example with $N_e = 40$ and element-by-element mass tailoring. The color band delimits a 10% of analytical error. Beyond the reduction of critical stepsize by half ($\alpha = 3$), the accuracy loss for lower modes is not permissible.

- System kinetic energy should be conserved after undergoing mass tailoring up to user-specified cut-off frequency defined as $\omega_c$.
- Modes and mode shapes of the low-frequency contents to be retained should not be modified.
- Tailored mass matrices should not require full dense matrix factorization.
- Tailored mass matrix should be applicable to all finite elements without requiring modifications FEM software within element generation routines. This can be taxing for nonlinear explicit transient analyses.
- Finally, it should avoid global tailoring (even though it can), which are typically are expensive and costly, especially for large-scale problems.

Mass matrix tailoring that satisfies most of the desirable properties set out above is described in the next section.

## 3 | PARTITIONED ANALYSIS

To derive the partitioned equations of motion of a linear structural dynamical system, we use the variational formulation proposed by Park and Felippa[24,25,23,26] where the problem is treated like if all bodies were entirely free. Then, the total virtual work of the complete system is obtained by summing up the contributions of each substructure, plus the contribution of the interface constraints via the method of localized Lagrange multipliers (LLM):

$$\delta\mathscr{W}_t = \delta\mathscr{W}_d + \delta\mathscr{W}_c \tag{6}$$

terms corresponding to the virtual work of the free-floating substructures and localized interface constraints, respectively.

The displacement-based discrete energy functional $\mathscr{W}_d(\mathbf{u})$, for a group of $N$ free-floating linear undamped substructures under dynamic loading, can be expressed in matrix form as:

$$\delta\mathscr{W}_d(\mathbf{u}) = \sum_{i=1}^{N} \delta\mathscr{W}_{d_i}(\mathbf{u}_i) = \sum_{i=1}^{N} \delta\mathbf{u}_i^{\mathsf{T}} \left\{\mathbf{M}_i\ddot{\mathbf{u}}_i + \mathbf{K}_i\mathbf{u}_i - \mathbf{f}_i\right\} = \delta\mathbf{u}^{\mathsf{T}} \left\{\mathbf{M}\ddot{\mathbf{u}} + \mathbf{K}\mathbf{u} - \mathbf{f}\right\} \tag{7}$$

with the following definitions,

$$\mathbf{M} = \begin{bmatrix} \mathbf{M}_1 & \cdots & \mathbf{0} \\ \vdots & \ddots & \vdots \\ \mathbf{0} & \cdots & \mathbf{M}_N \end{bmatrix}, \quad \mathbf{K} = \begin{bmatrix} \mathbf{K}_1 & \cdots & \mathbf{0} \\ \vdots & \ddots & \vdots \\ \mathbf{0} & \cdots & \mathbf{K}_N \end{bmatrix}, \quad \mathbf{u} = \begin{Bmatrix} \mathbf{u}_1 \\ \vdots \\ \mathbf{u}_N \end{Bmatrix}, \quad \mathbf{f} = \begin{Bmatrix} \mathbf{f}_1 \\ \vdots \\ \mathbf{f}_N \end{Bmatrix} \tag{8}$$

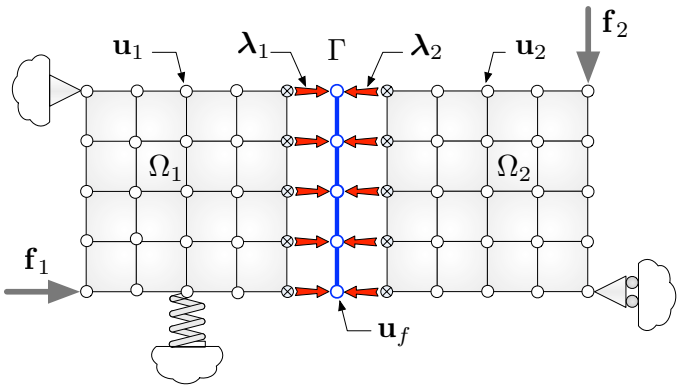


**FIGURE 2** Connection of two substructures using localized Lagrange multipliers. Localized Lagrange multipliers introduce an explicit definition of the interface with its own DOFs denominated frame.

where $\mathbf{u}$ is the partitioned subsystem-by-subsystem displacement vector, $\mathbf{f}$ the assembled vector of external forces, $\mathbf{K}$ and $\mathbf{M}$ are the block diagonal substructure-by-substructure stiffness and mass matrices, respectively, the subindex $i = 1, \ldots, N$ refers to partition number and the superscript dot denotes time differentiation.

The key to obtain a partitioned formulation of the problem is to treat the connection interfaces by the method of LLM that produces independent multipliers for each substructure. Specifically, see the case represented in Figure 2 with $N = 2$ partitions, instead of carrying out a direct coupling of the two bodies, we will introduce an explicit representation of the interface boundary $\Gamma$, denominated *frame*, with its own displacement DOFs $\mathbf{u}_f$, and consider the coupling in terms of interaction of the substructures with the frame.

We can write the substructure-frame boundary displacement compatibility equations as:

$$\mathbf{B}_i^{\mathsf{T}}\mathbf{u}_i = \mathbf{L}_{fi}\mathbf{u}_f \quad (i = 1 \cdots N) \quad \Rightarrow \quad \begin{Bmatrix} \mathbf{B}_1^{\mathsf{T}}\mathbf{u}_1 \\ \vdots \\ \mathbf{B}_N^{\mathsf{T}}\mathbf{u}_N \end{Bmatrix} = \begin{Bmatrix} \mathbf{L}_{f_1} \\ \vdots \\ \mathbf{L}_{f_N} \end{Bmatrix} \mathbf{u}_f \tag{9}$$

where $\mathbf{B}_i$ is the Boolean assembly matrix corresponding to $i^{th}$ substructure and $\mathbf{L}_{f_i}$ is the Boolean matrix relating the frame displacements $\mathbf{u}_f$ to the substructural displacements $\mathbf{u}_i$. These boundary constraints can be written in matrix form:

$$\mathbf{B}^{\mathsf{T}}\mathbf{u} - \mathbf{L}_f\mathbf{u}_f = \mathbf{0} \tag{10}$$

by making use of the block-matrices:

$$\mathbf{B} = \begin{bmatrix} \mathbf{B}_1 & \cdots & \mathbf{0} \\ \vdots & \ddots & \vdots \\ \mathbf{0} & \cdots & \mathbf{B}_N \end{bmatrix}, \quad \mathbf{L}_f = \begin{bmatrix} \mathbf{L}_{f_1} \\ \vdots \\ \mathbf{L}_{f_N} \end{bmatrix} \tag{11}$$

where $\mathbf{B}$ is the global boundary assembly operator and $\mathbf{L}_f$ is the frame-substructure interpolation matrix.

The partition interface constraint functional is simply obtained multiplying the boundary compatibility condition (10) by a field of Lagrange multipliers:

$$\mathscr{W}_{\mathrm{c}}\left(\mathbf{u}, \mathbf{u}_f, \lambda\right) = \lambda^{\mathsf{T}}\left\{\mathbf{B}^{\mathsf{T}}\mathbf{u} - \mathbf{L}_f\mathbf{u}_f\right\} \tag{12}$$

where $\lambda^{\mathsf{T}} = \left[\lambda_1^{\mathsf{T}} \cdots \lambda_N^{\mathsf{T}}\right]$ represents the independent LLMs of the substructures.

Finally, the total virtual work of the discrete partitioned system $\delta\mathscr{W}_t$ is derived combining (7) and (12) in the form:

$$\delta\mathscr{W}_t\left(\mathbf{u}, \mathbf{u}_f, \lambda\right) = \delta\mathbf{u}^{\mathsf{T}}\left\{\mathbf{M}\ddot{\mathbf{u}} + \mathbf{K}\mathbf{u} - \mathbf{f}\right\} + \delta\left\{\lambda^{\mathsf{T}}\left(\mathbf{B}^{\mathsf{T}}\mathbf{u} - \mathbf{L}_f\mathbf{u}_f\right)\right\} \tag{13}$$

and from the stationary-point condition of this virtual work, the partitioned equations of motion are obtained:

$$\begin{bmatrix} \mathbf{M} & \mathbf{B} & \mathbf{0} \\ \mathbf{B}^{\mathsf{T}} & \mathbf{0} & -\mathbf{L}_f \\ \mathbf{0} & -\mathbf{L}_f^{\mathsf{T}} & \mathbf{0} \end{bmatrix} \begin{Bmatrix} \ddot{\mathbf{u}} \\ \lambda \\ \ddot{\mathbf{u}}_f \end{Bmatrix} = \begin{Bmatrix} \mathbf{r} \\ \mathbf{0} \\ \mathbf{0} \end{Bmatrix} \tag{14}$$

with $\mathbf{r} = \mathbf{f} - \mathbf{K}\mathbf{u}$ and where all terms can be clearly identified; first equation represents the dynamic equilibrium of the elastic substructures, second equation imposes the interface constraint condition between the substructure boundaries and the frame, and last equation imposes the frame equilibrium condition.

It is here, at the partition level, that we propose a modification of the mass matrices, replacing the original partitioned mass matrix $\mathbf{M}$ by a substructure by substructure modified mass matrix $\hat{\mathbf{M}}$, specifically designed to satisfy the requirements enumerated in the previous section.

*Remark 1.* Once the modification of the mass matrices has been performed at the substructure level, the problem could be solved in a monolithic way by reassembling the partitioned matrices into a global equation, maintaining displacements as the only unknowns. However, this is not always practical, specially for problems with a large number of DOFs.

## 3.1 | Partitioned explicit time marching algorithm

As observed in Section 2, while it is easy to implement elemental mass tailoring (EMT), for most finite elements EMT does restrict the stepsize gain due to accuracy loss. On the other hand, global mass tailoring (GMT) can be computational expensive, especially for problems where the number of mesh frequency modes are excessively large. Hence, we will employ partitioned (substructural) mass tailoring (PMT) that offers the following features:

- The number of mesh frequencies to be tailored in each partition are substantially smaller than those in global structures;
- For structures consisting of heterogeneous substructures, different mass tailoring can be applied to each partition. This feature is especially attractive for explicit time marching of multiphysics problems.

To this end, consider the substructure-by-substructure partitioned equation (14) with the mass matrix ($\mathbf{M}$) replaced by a modified mass matrix ($\hat{\mathbf{M}}$):

$$\begin{bmatrix} \hat{\mathbf{M}} & \mathbf{B} & \mathbf{0} \\ \mathbf{B}^{\mathsf{T}} & \mathbf{0} & -\mathbf{L}_f \\ \mathbf{0} & -\mathbf{L}_f^{\mathsf{T}} & \mathbf{0} \end{bmatrix} \begin{Bmatrix} \ddot{\mathbf{u}} \\ \lambda \\ \ddot{\mathbf{u}}_f \end{Bmatrix} = \begin{Bmatrix} \mathbf{r} \\ \mathbf{0} \\ \mathbf{0} \end{Bmatrix} \tag{15}$$

where $\left(\ddot{\mathbf{u}}, \lambda, \ddot{\mathbf{u}}_f\right)$ are the substructural accelerations, substructural interface forces and the frame accelerations, respectively. Now, the partitioned (or substructure-by-substructure) accelerations are isolated from the first equation:

$$\ddot{\mathbf{u}} = \hat{\mathbf{M}}^{-1}\left(\mathbf{r} - \mathbf{B}\lambda\right) \tag{16}$$

and substituted into the second equation:

$$\mathbf{B}^{\mathsf{T}}\hat{\mathbf{M}}^{-1}\left(\mathbf{r} - \mathbf{B}\lambda\right) - \mathbf{L}_f\ddot{\mathbf{u}}_f = \mathbf{0} \tag{17}$$

to yield the system:

$$\begin{bmatrix} \mathbf{B}^{\mathsf{T}}\hat{\mathbf{M}}^{-1}\mathbf{B} & \mathbf{L}_f \\ \mathbf{L}_f^{\mathsf{T}} & \mathbf{0} \end{bmatrix} \begin{Bmatrix} \lambda \\ \ddot{\mathbf{u}}_f \end{Bmatrix} = \begin{Bmatrix} \mathbf{b} \\ \mathbf{0} \end{Bmatrix} \tag{18}$$

with $\mathbf{b} = \mathbf{B}^{\mathsf{T}}\hat{\mathbf{M}}^{-1}\mathbf{r}$, from where we can compute the interface unknowns.

To describe the explicit time marching scheme, see Algorithm 1, suppose that computations have proceeded until $t = t^n$ and we seek a solution for $t^{n+1} = t^n + \Delta t$. Then, time integration proceeds as follows. First, the interface forces $\lambda^n$ are computed solving (18). This step can be performed iteratively[27] or in a direct form as described in Algorithm 1, solving first for the frame accelerations $\ddot{\mathbf{u}}_f^n$ and then for the multipliers $\lambda^n$. Once we know the interface forces, the accelerations $\ddot{\mathbf{u}}^n$ are obtained from (16). Finally, updating of the velocity and displacement can be made via the summed form of the central difference method:

$$\begin{cases} \dot{\mathbf{u}}^{n+\frac{1}{2}} = \dot{\mathbf{u}}^{n-\frac{1}{2}} + \Delta t\, \ddot{\mathbf{u}}^n \\ \mathbf{u}^{n+1} = \mathbf{u}^n + \Delta t\, \dot{\mathbf{u}}^{n+\frac{1}{2}} \end{cases} \tag{19}$$

and we are ready to proceed with the next time step.

In employing the partitioned explicit integration procedure outlined above, there are two mass tailoring procedures: high-frequency filtering procedure and low-frequency mode preservation procedure. Both techniques are described below.

**Algorithm 1** Partitioned explicit time integration by central difference scheme

$\mathbf{u}^0, \dot{\mathbf{u}}^0, \dot{\mathbf{u}}^{\frac{1}{2}} = \dot{\mathbf{u}}^0 + \frac{\Delta t}{2}\ddot{\mathbf{u}}^0$ ▷ Initial conditions

**for** n **do** 1...$n$ **time loop** ▷ Time integration loop

$\mathbf{r}^n = \mathbf{f}^n - \mathbf{K}\mathbf{u}^n$ ▷ Evaluate residual forces

$\mathbf{b}^n = \mathbf{B}^\top \hat{\mathbf{M}}^{-1}\mathbf{r}^n$ ▷ Evaluate free term

$\left[\mathbf{L}_f^\top \left(\mathbf{B}^\top \hat{\mathbf{M}}^{-1}\mathbf{B}\right)^{-1} \mathbf{L}_f\right] \ddot{\mathbf{u}}_f^n = \left\{\mathbf{L}_f^\top \mathbf{b}^n\right\}$ ▷ Solve for frame accelerations $\ddot{\mathbf{u}}_f^n$

$\left[\mathbf{B}^\top \hat{\mathbf{M}}^{-1}\mathbf{B}\right] \lambda^n = \left\{\mathbf{b}^n - \mathbf{L}_f \ddot{\mathbf{u}}_f^n\right\}$ ▷ Solve for interface forces $\lambda^n$

$\ddot{\mathbf{u}}^n = \hat{\mathbf{M}}^{-1}\left(\mathbf{r}^n - \mathbf{B}\lambda^n\right)$ ▷ Compute global accelerations

$\dot{\mathbf{u}}^{n+\frac{1}{2}} = \dot{\mathbf{u}}^{n-\frac{1}{2}} + \Delta t \ddot{\mathbf{u}}^n$ ▷ Update global velocities

$\mathbf{u}^{n+1} = \mathbf{u}^n + \Delta t \dot{\mathbf{u}}^{n+\frac{1}{2}}$ ▷ Update global displacements

**end for** ▷ Proceed to the next time step

## 4 | MASS TAILORING EMPLOYING HIGH-FREQUENCY MODE SHAPES WITH A CUT-OFF FREQUENCY

We start examining the original mode shapes of a substructure, that are obtained by solving the generalized eigenvalue problem:

$$\mathbf{K}\boldsymbol{\Phi} = \mathbf{M}\boldsymbol{\Phi}\boldsymbol{\Lambda} \tag{20}$$

with the well known eigen-decomposition properties,

$$\begin{cases} \boldsymbol{\Phi}^\top \mathbf{K}\boldsymbol{\Phi} = \boldsymbol{\Lambda} \\ \boldsymbol{\Phi}^\top \mathbf{M}\boldsymbol{\Phi} = \mathbf{I}_n \end{cases} \tag{21}$$

where $\boldsymbol{\Phi} \in \mathbb{R}^{n\times n}$ is a square matrix with the orthogonal mode shapes of the substructure, $\mathbf{I}_n$ is the identity matrix of size $n$ and the diagonal matrix $\boldsymbol{\Lambda} \in \mathbb{R}^{n\times n}$ contains the original system eigenfrequencies, i.e., $\boldsymbol{\Lambda} = \mathbf{diag}\left[\omega_1^2, \omega_2^2 \dots \omega_n^2\right]$.

Then, after ordering the frequencies in $\boldsymbol{\Lambda}$, the $n$ orthogonal mode shapes can be separated into $r$ and $m = n - r$ low and high frequency mode shapes, respectively, in the form:

$$\boldsymbol{\Phi} = \left[\boldsymbol{\Phi}_l \;\; \boldsymbol{\Phi}_h\right] \tag{22}$$

where $\boldsymbol{\Phi}_l \in \mathbb{R}^{n\times r}$ groups low-frequency modes whose responses are to be retained and $\boldsymbol{\Phi}_h \in \mathbb{R}^{n\times m}$ collects high-frequency modes whose responses are to be filtered out. These orthogonal modes now fulfill,

$$\boldsymbol{\Lambda} = \begin{bmatrix} \boldsymbol{\Phi}_l^\top \mathbf{K}\boldsymbol{\Phi}_l & \mathbf{0} \\ \mathbf{0} & \boldsymbol{\Phi}_h^\top \mathbf{K}\boldsymbol{\Phi}_h \end{bmatrix} = \begin{bmatrix} \boldsymbol{\Lambda}_l & \mathbf{0} \\ \mathbf{0} & \boldsymbol{\Lambda}_h \end{bmatrix} \tag{23}$$

where $\boldsymbol{\Lambda}_l \in \mathbb{R}^{r\times r}$ and $\boldsymbol{\Lambda}_h \in \mathbb{R}^{m\times m}$ are diagonal matrices grouping with the corresponding low and high frequencies.

### 4.1 | High-frequency based mass matrix tailoring

First, we adopt the elemental mass tailoring introduced in (4) to partitioned substructural mass matrices, $\hat{\mathbf{M}}_h$:

$$\hat{\mathbf{M}}_h = \mathbf{M} + \mathbf{M}\boldsymbol{\Phi}_h \mathbf{S}_h \boldsymbol{\Phi}_h^\top \mathbf{M}, \tag{24}$$

using the diagonal tailoring matrix,

$$\mathbf{S}_h = \mathbf{diag}\left[s_1, s_2 \dots s_m\right] \tag{25}$$

where $\boldsymbol{\Phi}_h \in \mathbb{R}^{n\times m}$ is now a retained set of higher mode shapes whose frequencies are deemed to be mesh frequencies and therefore to be filtered out; $\mathbf{S}_h \in \mathbb{R}^{m\times m}$ is a diagonal matrix to be discussed subsequently and $m$ is the number of the higher mode shapes utilized.

**Proposition 1.** The tailored mass matrix $\hat{\mathbf{M}}_h$ scales the high frequencies of the partition by a factor $(\mathbf{I}+\mathbf{S})^{-1}$, maintaining the partition low frequencies unaffected, i.e., the new tailored partition eigenvalues are given by the diagonal matrix:

$$\hat{\mathbf{\Lambda}}_h = \begin{bmatrix} \mathbf{I}_r & \mathbf{0} \\ \mathbf{0} & (\mathbf{I}_m + \mathbf{S}_h)^{-1} \end{bmatrix} \mathbf{\Lambda}$$

with the same mode shapes $\mathbf{\Phi}$ of the original partitioned system.

*Proof.* It is very simple to demonstrate that the new tailored-mass eigenvalue problem:

$$\mathbf{K}\mathbf{\Phi} = \hat{\mathbf{M}}_h \mathbf{\Phi} \hat{\mathbf{\Lambda}}_h$$

has exactly the same eigenvectors than the original one, with the same $r$ low frequencies and $s$ reduced high frequencies. This is demonstrated premultiplying by $\mathbf{\Phi}^{\mathsf{T}}$ the previous expression, thanks to properties (21), revealing the new eigenvalues:

$$\mathbf{\Lambda} = \mathbf{\Phi}^{\mathsf{T}} \left( \mathbf{M} + \mathbf{M} \begin{bmatrix} \mathbf{\Phi}_l & \mathbf{\Phi}_h \end{bmatrix} \begin{bmatrix} \mathbf{0} & \mathbf{0} \\ \mathbf{0} & \mathbf{S}_h \end{bmatrix} \begin{bmatrix} \mathbf{\Phi}_l & \mathbf{\Phi}_h \end{bmatrix}^{\mathsf{T}} \mathbf{M} \right) \mathbf{\Phi} \hat{\mathbf{\Lambda}}_h = \left( \mathbf{I}_n + \begin{bmatrix} \mathbf{0} & \mathbf{0} \\ \mathbf{0} & \mathbf{S}_h \end{bmatrix} \right) \hat{\mathbf{\Lambda}}_h$$

from where we can obtain $\hat{\mathbf{\Lambda}}_h$ inverting a simple diagonal matrix. □

## 4.2 | Design of the tailoring matrix

We seek now an expression for the tailoring matrix (25). Of several possible choices to construct $\mathbf{S}_h$, we propose the following formula:

$$\mathbf{S}_h = \tfrac{1}{\omega_c^2} \mathbf{\Lambda}_h - \mathbf{I}_m \tag{26}$$

where $\omega_c$ is a user-specified cut-off frequency beyond which all the higher frequencies will be filtered out. Substituting (26) in the result of Proposition 1, we observe that the modified frequencies take the form:

$$\hat{\mathbf{\Lambda}}_h = \begin{bmatrix} \mathbf{\Lambda}_l & \mathbf{0} \\ \mathbf{0} & \omega_c^2 \mathbf{I}_m \end{bmatrix}. \tag{27}$$

It is observed from the preceding result that, while the lower modes ($\mathbf{\Lambda}_l$) and their mode shapes of each substructure are preserved, the higher modes which are expected to consist of mesh frequencies are effectively filtered out and replaced by the cut-off frequency, $\omega_c$. One can show that the mass tailoring matrix given by (26) satisfies the first five desirable properties. As for the sixth desirable property, while depending on existing elemental mass matrix routines, a substructural-level modification is necessary. This can be implemented as part of solution strategies.

## 4.3 | Implementation details for high-frequency modes mass tailoring

For computational efficiency, $\hat{\mathbf{M}}_h^{-1}$ can be explicitly given via the well-known Woodbury formula[28]:

$$\hat{\mathbf{M}}_h^{-1} = \mathbf{M}^{-1} - \mathbf{\Phi}_h \left( \mathbf{S}_h^{-1} + \mathbf{I}_m \right)^{-1} \mathbf{\Phi}_h^{\mathsf{T}} \tag{28}$$

where $\mathbf{\Phi}_h^{\mathsf{T}} \mathbf{M} \mathbf{\Phi}_h = \mathbf{I}_m$ is utilized. Hence, if the tailoring matrix $\mathbf{S}_h$ is diagonal then $\hat{\mathbf{M}}^{-1}$ is trivially obtained, especially when employing a diagonal partitioned mass matrix. Note also that many prefer to use a diagonal mass matrix for explicit time integration.

Solution of $\lambda$ in (18) is straightforward in itself. If desired, one can use the following predictor-corrector form or iterative form:

$$\begin{bmatrix} \mathbf{B}^{\mathsf{T}} \mathbf{M}^{-1} \mathbf{B} & \mathbf{L}_f \\ \mathbf{L}_f^{\mathsf{T}} & \mathbf{0} \end{bmatrix} \begin{Bmatrix} \lambda_k^n \\ \ddot{\mathbf{u}}_f \end{Bmatrix} = \begin{Bmatrix} \mathbf{b}^n + \mathbf{B}^{\mathsf{T}} \left[ \mathbf{\Phi}_h \left( \mathbf{S}_h^{-1} + \mathbf{I}_m \right)^{-1} \mathbf{\Phi}_h^{\mathsf{T}} \right] \mathbf{B} \lambda_{k-1}^n \\ \mathbf{0} \end{Bmatrix} \tag{29}$$

Observe that, since $\mathbf{M}$ is diagonal, the matrices $\mathbf{B}^{\mathsf{T}} \mathbf{M}^{-1} \mathbf{B}$ and $\mathbf{L}_f^{\mathsf{T}} \left( \mathbf{B}^{\mathsf{T}} \mathbf{M}^{-1} \mathbf{B} \right)^{-1} \mathbf{L}_f$ needed in the predictor-corrector iteration, are also diagonal.

### 4.4 | Stepsize gain

Adoption of the tailoring matrix given by (27) offers the following stepsize gain:

$$\mathsf{N}_{\text{gain}} = \frac{\omega_{max}}{\omega_c} = \frac{\Delta t_t}{\Delta t_{max}} \tag{30}$$

where $\left(\Delta t_t, \Delta t_{max}\right)$ are the maximum table stepsize for the mass tailored case and the original partitioned system, respectively. It will be shown that a stepsize gain of 5 to 10 are within the manageable gain levels for most low-frequency dominated explicit transient analysis cases.

## 5 | MASS TAILORING EMPLOYING LOW-FREQUENCY MODE SHAPES

In the previous Section, the basic mass tailoring tools were the high-frequency substructural mode shapes $\mathbf{\Phi}_h$ with its associated frequencies $\mathbf{\Lambda}_h$ limited by a cut-off frequency $\omega_c$. But, there are cases for some substructures where we need to compute an excessive number of high-frequency mode shapes. In this case, it is preferable to perform the mass tailoring using the low-frequency mode shapes $\mathbf{\Phi}_l$. For such a case, we compute low-frequency mode shapes and construct a new tailored mass matrix $\hat{\mathbf{M}}_l$ as follows:

$$\hat{\mathbf{M}}_l = \mathbf{M} + \mathbf{P}_l^{\mathsf{T}} \mathbf{S}_l \mathbf{P}_l \tag{31}$$

with a new tailoring matrix,

$$\mathbf{S}_l = \tfrac{1}{\omega_c^2}\mathbf{K} - \mathbf{M} \tag{32}$$

and a projection operator constructed using the lower-modes:

$$\mathbf{P}_l = \mathbf{I} - \mathbf{\Phi}_l \mathbf{\Phi}_l^{\mathsf{T}} \mathbf{M} \tag{33}$$

where $\mathbf{P}_l \in \mathbb{R}^{n\times n}$ is a projector that filters out the lower modes leaving the higher modes unaffected, i.e., $\mathbf{P}_l\mathbf{\Phi} = \begin{bmatrix}\mathbf{0} & \mathbf{\Phi}_h\end{bmatrix}$. In this case, $\mathbf{\Phi}_l \in \mathbb{R}^{n\times r}$ is selected as a set of $r$ lower mode shapes whose frequencies are deemed to be the dominant response frequencies of the system and therefore to be retained.

**Proposition 2.** The tailored mass matrix $\hat{\mathbf{M}}_l$ scales the high frequencies of the partition to $\omega_c^2$, maintaining the partition low frequencies unaffected, i.e., the new partition eigenvalues are given by the diagonal matrix:

$$\hat{\mathbf{\Lambda}}_l = \begin{bmatrix}\mathbf{I}_r & \mathbf{0} \\ \mathbf{0} & \omega_c^2 \mathbf{\Lambda}_h^{-1}\end{bmatrix} \mathbf{\Lambda}$$

with the same modes $\mathbf{\Phi}$ than the original unscaled partition.

*Proof.* As we did before, we multiply by $\mathbf{\Phi}^{\mathsf{T}}$ the new tailored-mass eigenvalue problem:

$$\mathbf{K\Phi} = \hat{\mathbf{M}}_l \mathbf{\Phi} \hat{\mathbf{\Lambda}}_l$$

to obtain the relation between the original and the new eigenvalues:

$$\mathbf{\Lambda} = \left(\mathbf{I}_n + \begin{bmatrix}\mathbf{0} & \mathbf{\Phi}_h\end{bmatrix} \mathbf{S}_l \begin{bmatrix}\mathbf{0} & \mathbf{\Phi}_h\end{bmatrix}^{\mathsf{T}}\right) \hat{\mathbf{\Lambda}}_l = \left(\mathbf{I}_n + \begin{bmatrix}\mathbf{0} & \mathbf{0} \\ \mathbf{0} & \frac{1}{\omega_c^2}\mathbf{\Lambda}_h\end{bmatrix}\right) \hat{\mathbf{\Lambda}}_l$$

from where we can isolate the expression for $\hat{\mathbf{\Lambda}}_l$ . □

Comparing the tailored frequencies $\hat{\mathbf{\Lambda}}_h$ obtained by employing the high-frequency mode shapes (24) and $\hat{\mathbf{\Lambda}}_l$ obtained by employing the low-frequency mode shapes (31), it is seen that both tailoring procedures lead to the same modified frequency distributions, viz.,

$$\hat{\mathbf{\Lambda}}_h = \hat{\mathbf{\Lambda}}_l = \begin{bmatrix}\mathbf{\Lambda}_l & \mathbf{0} \\ \mathbf{0} & \omega_c^2 \mathbf{I}\end{bmatrix}. \tag{34}$$

It is noted that, even if one has to invert the dense substructural mass matrix, it may be still attractive especially for most stiff partitions since filtering all the higher modes may be computationally excessive.

**Algorithm 2** Efficient procedure for the computation of the stiffness matrix generalized inverse $\mathbf{K}^{+}$.

$$\mathbf{R} = \begin{bmatrix} \mathbf{R}_c \\ \mathbf{R}_f \end{bmatrix}, \qquad \mathbf{K} = \begin{bmatrix} \mathbf{K}_{cc} & \mathbf{K}_{cf} \\ \mathbf{K}_{fc} & \mathbf{K}_{ff} \end{bmatrix} \qquad \triangleright \text{ Partition rigid-body mode shape and substructural stiffness matrices}$$

$$\bar{\mathbf{R}} = \mathbf{R}_f \mathbf{R}_c^{-1} \;\Rightarrow\; \mathbf{T} = \begin{bmatrix} -\bar{\mathbf{R}} & \mathbf{I} \end{bmatrix} \qquad \triangleright \text{ Construct matrices } \bar{\mathbf{R}} \text{ and } \mathbf{T}$$

$$\mathbf{D}_r = \mathbf{I}_{n_r} - \bar{\mathbf{R}} \left[ \mathbf{I} + \bar{\mathbf{R}}^{\mathsf{T}} \bar{\mathbf{R}} \right]^{-1} \bar{\mathbf{R}} \qquad \triangleright \text{ Compute matrix } \mathbf{D}_r$$

$$\mathbf{K}^{+} = \mathbf{T}^{\mathsf{T}} \mathbf{D}_r \, \mathbf{K}_{ff}^{-1} \, \mathbf{D}_r \mathbf{T} \qquad \triangleright \text{ Obtain pseudo-inverse } \mathbf{K}^{+}$$

## 5.1 | Implementation details for low-frequency modes mass tailoring

A direct inverse of the low-frequency modification (31) for explicit transient analysis leads to full matrix inversion. Once again, the Woodbury formula should be invoked to arrive at the following inverse mass matrix:

$$\hat{\mathbf{M}}_l^{-1} = \omega_c^2 \mathbf{K}^{-1} + \boldsymbol{\Phi}_l \mathbf{C}_l \boldsymbol{\Phi}_l^{\mathsf{T}}, \tag{35}$$

with a diagonal matrix,

$$\mathbf{C}_l = \mathbf{I}_r - \omega_c^2 \boldsymbol{\Lambda}_l^{-1} \tag{36}$$

that can be easily computed.

**Proposition 3.** Tailored inverse mass matrices (28) and matrix (35) are completely equivalent. They represent the same expression obtained via higher modes or lower modes, respectively.

*Proof.* We start incorporating the proposed scaling (26) into the tailored inverse with higher modes (28) and compute the inverse of the diagonal matrix to obtain:

$$\hat{\mathbf{M}}_h^{-1} = \mathbf{M}^{-1} - \boldsymbol{\Phi}_h \left( \mathbf{I}_m - \omega_c^2 \boldsymbol{\Lambda}_h^{-1} \right) \boldsymbol{\Phi}_h^{\mathsf{T}}$$

and then substitute the decomposition of the inverse mass matrix into lower and higher modes, i.e., $\mathbf{M}^{-1} = \boldsymbol{\Phi}_l \mathbf{I}_r \boldsymbol{\Phi}_l^{\mathsf{T}} + \boldsymbol{\Phi}_h \mathbf{I}_m \boldsymbol{\Phi}_h^{\mathsf{T}}$, to find the following relation:

$$\hat{\mathbf{M}}_h^{-1} = \boldsymbol{\Phi}_l \mathbf{I}_r \boldsymbol{\Phi}_l^{\mathsf{T}} + \omega_c^2 \boldsymbol{\Phi}_h \boldsymbol{\Lambda}_h^{-1} \boldsymbol{\Phi}_h^{\mathsf{T}}$$

where higher modes only appear in the second term. Next, we use the decomposition for the stiffness matrix inverse $\mathbf{K}^{-1} = \boldsymbol{\Phi}_l \boldsymbol{\Lambda}_l^{-1} \boldsymbol{\Phi}_l^{\mathsf{T}} + \boldsymbol{\Phi}_h \boldsymbol{\Lambda}_h^{-1} \boldsymbol{\Phi}_h^{\mathsf{T}}$ to eliminate these higher modes and write:

$$\hat{\mathbf{M}}_h^{-1} = \boldsymbol{\Phi}_l \mathbf{I}_r \boldsymbol{\Phi}_l^{\mathsf{T}} + \omega_c^2 \left( \mathbf{K}^{-1} - \boldsymbol{\Phi}_l \boldsymbol{\Lambda}_l^{-1} \boldsymbol{\Phi}_l^{\mathsf{T}} \right) = \hat{\mathbf{M}}_l^{-1}$$

arriving finally to equation (35). □

Since matrix $\mathbf{C} \in \mathbb{R}^{r \times r}$ is diagonal, one only needs to factorize the substructural stiffness matrix $\mathbf{K}$. It should be noted that $\mathbf{K}^{-1}$ should be replaced by its pseudo-inverse when the substructures are floating. For this case, an efficient procedure exists[24], which is reproduced in Algorithm 2, where $\left(\mathbf{R}_c, \mathbf{K}_{ff}\right)$ are square matrices which have their corresponding full ranks as they should be and the intermediate matrix $\mathbf{D}_r \in \mathbb{R}^{n_r \times n_r}$, where $n_r$ is the number of rigid body modes, which maximum dimension is 6 for three displacements and three rotations in $\mathbb{R}^3$.

The preceding mass tailoring employing the substructural low-frequency mode shapes also fulfills the first five desirable properties set out in Section 2.2.

## 5.2 | When is the mass tailoring employing low-frequency mode shapes desirable?

It is noted that the mass tailoring employing low-frequency mode shapes requires the inversion (or generalized inverse) of substructural stiffness matrix as seen from (35). Hence, adoption of this tailoring should be sparingly employed. One notable case is when a substructure is much more stiff compared with the rest of the partitions, whose mesh frequencies would be larger. We will defer a trade-off study between the high-frequency vs low-frequency mass tailoring to a later occasion.

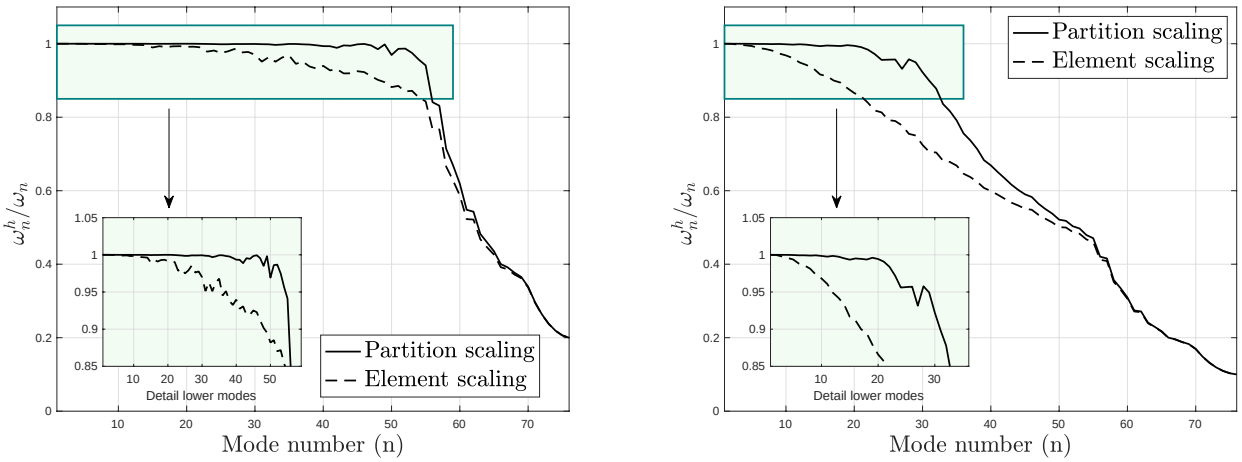


**FIGURE 3** Tailoring of substructural mass matrix for one-dimensional bar example for step size increase by a factor $\mathsf{N}_{\text{gain}} = 5$ and $\mathsf{N}_{\text{gain}} = 10$, respectively. Error in the global frequencies.

## 6 | ADVANTAGE OF EMPLOYING THE SUBSTRUCTURAL CUT-OFF FREQUENCY IN LIEU OF THE GLOBAL CUT-OFF FREQUENCY

There is an important property we should mention. That is, what about the global cut-off frequency?... the answer to this question comes from the classical eigenvalue bounding property of finite element stiffness and mass matrices that goes back to the early 1970s. If all the substructural mass matrices are modified in a similar manner, with the same cut-off frequency, then B. Iron's bounding theorem[29,30] states that the maximum frequency of the assembled system is bounded by the maximum frequency of elemental-substructural maximum frequencies. As the present mass tailoring employs the same cut-off frequency for all substructures, the maximum frequency of the assembled system is bounded by $\omega_c$. This leads us to use the maximum stable explicit stepsize given by:

$$\Delta t_c = \frac{2}{\omega_c} \; > \; \Delta t_s = \frac{2}{\omega_{max}}, \quad \omega_{max} = \max\left(\omega_{max,1}, \omega_{max,2} \ldots \omega_{max,N}\right) \tag{37}$$

where $\omega_{max,i}$ is the maximum frequency for the i$^{th}$ partition substructure. Therefore, we can define the *stepsize gain factor*,

$$\boxed{\mathsf{N}_{\text{gain}} = \frac{\Delta t_c}{\Delta t_s}} \tag{38}$$

as the critical time stepsize extension we have obtained for explicit time integration thanks to the scaling process.

It is important to mention that, although different mass-tailoring methods have been proposed by other authors[13,16,17], the proposed mass-tailoring technique is defined as selective in the sense that we can choose the number of modes to be filtered out or retained and this tailoring is performed at the *substructural* level or *elemental* level when doing so would yield the overall accuracy to be maintained.

## 7 | NUMERICAL EXPERIMENTS

In this section, we test the proposed mass tailoring technique via eigenvalue analysis, using the scaled mass matrices as compared with the unscaled consistent mass matrices. This is done for different finite element types.

**TABLE 2** Input data used in example bar problems shown in Figure 3 .

| | | Partition | | | | |
|---|---|---|---|---|---|---|
| **Property** | **Units** | $i = 1$ | $i = 2$ | $i = 3$ | $i = 4$ | $i = 5$ |
| Density | $kg/m^3$ | 3000 | 1500 | 1000 | 2000 | 3000 |
| Elastic modulus | kPa | 10 | 20 | 10 | 30 | 3 |
| Cross section | $cm^2$ | 50 | 50 | 50 | 50 | 50 |
| Element size | cm | 0.1 | 1 | 1 | 1 | 0.1 |
| Number of elements | – | 15 | 15 | 15 | 15 | 15 |

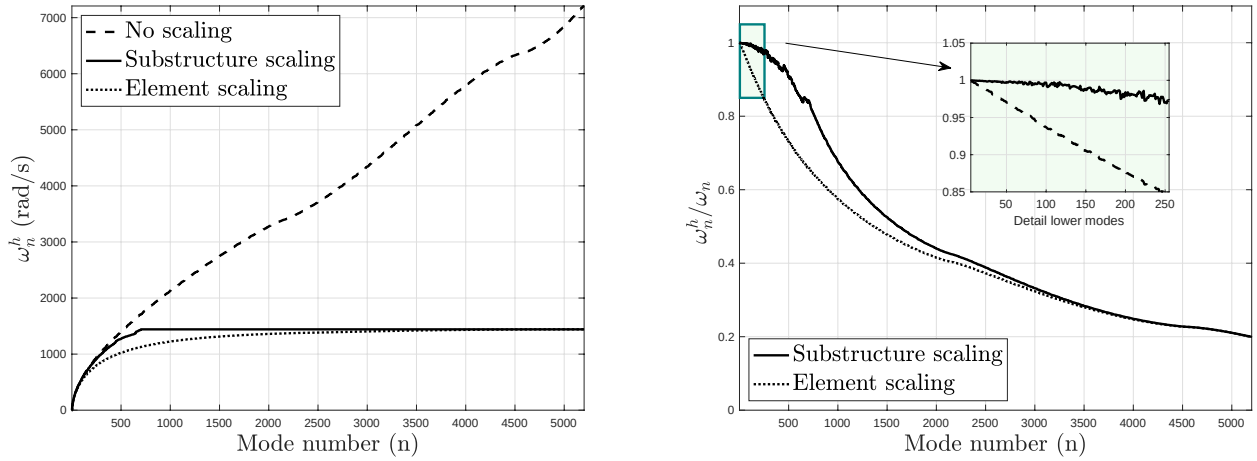


**FIGURE 4** Tailoring of plane stress vibration problem by the present tailoring of substructural mass matrix, achieving a stepsize increase by stesize gain factor $\mathsf{N}_{\text{gain}} = 5$.

## 7.1 | One-dimensional bar problem

As shown in Section 2, elemental mass matrix tailoring yields at most an increase of the step size by the factor $\mathsf{N}_{\text{gain}} = 2$ due to accuracy restrictions. Figure 3 illustrates a bar example with 5 substructures consisting of 15 elements per each substructure, with varying lengths, densities and Young's modulus shown in Table 2 .

When the step size increase by the stepsize gain factor $\mathsf{N}_{\text{gain}} = 5$ compared with non-scaled mass matrices is desired, the accuracy of the elemental tailoring case starts to deteriorate after 10 modes. The substructural mass matrix tailoring employing the high-frequency mode shapes (24) continues to yield good accuracy for modes up to 40 modes. When the step size increase by $\mathsf{N}_{\text{gain}} = 10$ is sought, however, elemental tailoring start to lose accuracy after a few modes whereas the substructural mass tailoring offers good accuracy up to a dozen modes.

## 7.2 | Plane stress vibration problem

We now move on to the task of plain stress frequency filtering. In order to assess the proposed mass tailoring method, viz., higher-mode shape based method (27) and the lower-mode shaped based method (31) beyond the one-dimensional problem. To this end, a square domain $\Omega \in [0, 1]^2$ with $5 \times 5$ partitions, with each partition modeled by $10 \times 10$ elements. Subdomain size is $H = 1/5$ and element size $h = H/10$. For the material properties, the elasticity modulus of $E = 1$ MPa, Poisson's ratio of $\nu = 0.3$ and the density of $\rho = 1000\,\text{kg/m}^3$ are used.

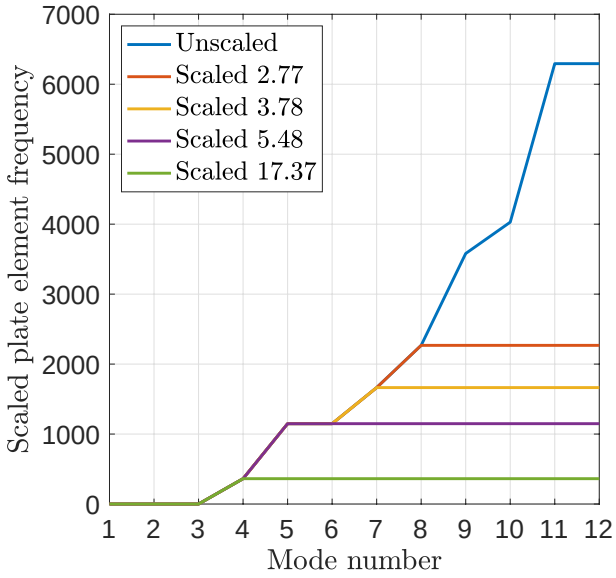


**FIGURE 5** Elemental tailoring of plate bending mass matrix by the present tailoring with three different cut-off frequencies.

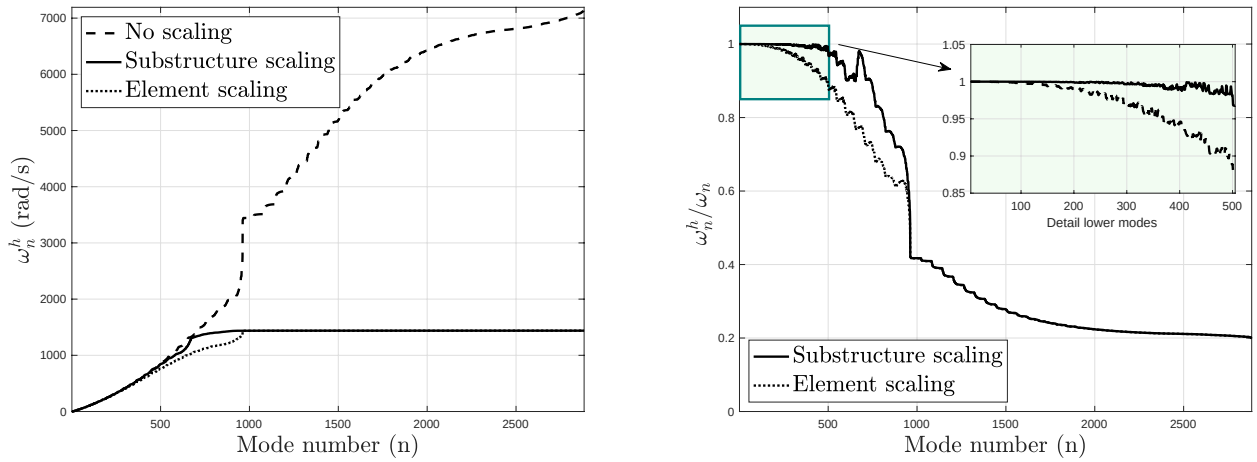


**FIGURE 6** Tailoring of plate vibration problem by the present tailoring of substructural mass matrix, achieving a step size increase by stepsize gain factor $\mathsf{N}_{\mathsf{gain}} = 5$. Plate is discretized by $36 \times 36$ 4-node bending element, with each partition consisting of 36 elements.

The global problem has 5, 202 DOFs and each substructure consists of 242 DOFs. For each substructure, 28 lower modes are used for the tailoring to increase the critical stepsize by a factor of 5. Results are presented in Figure 4 . We have also performed the same eigenvalue analysis employing the higher-mode method, requiring 214 higher mode shapes, with identical result. On the other hand, element by element scaling requires modification of the 5 higher element frequencies. For this problem, it is clear that elemental mass tailoring yields poor performance in spite of using a larger number of higher modes.

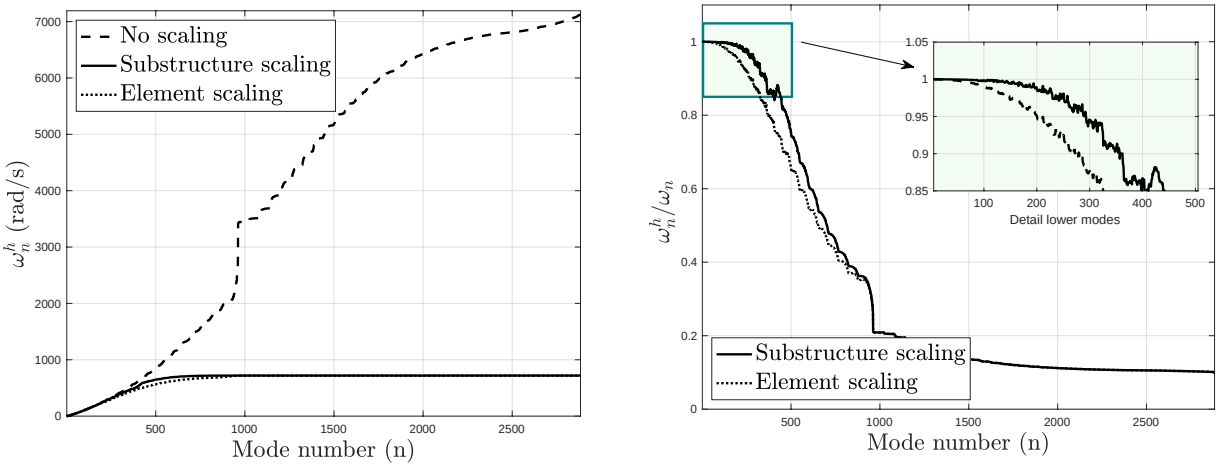


**FIGURE 7** Tailoring of plate vibration problem by the present tailoring of substructural mass matrix, achieving a step size increase by stepsize gain factor $\mathsf{N}_{\mathsf{gain}} = 10$. The plate is discretized by $36 \times 36$ quadrilateral 4-node bending element, with each partition consisting of 9 elements.

## 7.3 | Plate bending vibration problem

Explicit transient analysis of plates and shells presents a different challenge compared with problems modeled with plain stress elements and three-dimensional solid elements. This is because due to high frequencies associated with transverse shear, out-of-plane rotational modes and in-plane membrane modes relative to bending modes. Thus, one is tempted to apply the present proposed mass tailoring methods to elemental mass tailoring.

Figure 5 shows the performance of the present mass tailoring as applied to a single free-free plate bending element by filtering the 6, 5 and 4 higher modes, respectively. As expected, the present methods preserve the first non-zero 3, 4 and 5 low modes and their corresponding elemental mode shapes are preserved, achieving an increase of critical step size by a factor of 5.48, 3.78, 2.77, respectively. The first three elemental non-zero mode shapes are a diagonally bending mode, two x and y-directional beam bending modes, and the fourth and fifth are fundamental shear mode, which is desirable to be included for accuracy consideration. Hence, employing elemental mass tailoring, the most one can achieve is the step size increase by a factor of 3.78 from the accuracy viewpoint. Of course, one can deliberately accomplish the step size by a factor of 5.48 by taking the cut-off frequency to coincide with the third elemental bending mode.

With the insight gained from elemental tailoring employing the present tailoring methods, a large-scale problem of plate problems consisting of $\Omega \in [0, 1]^2$ with $5 \times 5$ partitions, with each partition having $6 \times 6$ elements. Subdomain size is $H = 1/5$ and element size $h = H/6$. For the material properties, values of elasticity modulus $E = 1$ MPa, Poisson's ratio $\nu = 0.3$, thickness $t = 0.01$ m and density $\rho = 1000\,\mathrm{kg/m^3}$ are used.

The global problem has 2, 283 DOFs and each substructure presents 147 DOFs. Mass tailoring, to achieve the critical time-step of 5 times larger than by the original plate mass matrix, required 44 lower modes using equation (31) or 103 higher modes with equation (24). The results are presented in Figure 6.

In order to assess the sensitivity of substructural sizes on the number of mode shapes (either low modes or higher mode shapes), the same plate is now partitioned into 100 substructural partitions from 25 partitions. For this refined partitions, 9 mode shapes do the job of attaining 10 times increase of the unscaled critical step size as shown in Figure 7.

## 7.4 | Transient analysis of a cantilever beam under tip load

To test the solid hexahedral element, we use the cantilever beam with vertical load proposed Olovsson et al. in[10] also studied by Tkachuk et al.[16,19] to investigate the accuracy of variational mass scaling methods. The geometrical definition of the problem is shown in Figure 8, where a cantilever beam of length $L = 0.1$ m and section height $b = 0.003$ m with thickness $t = 0.001$ m is considered. Material properties of the beam are $E = 207$ GPa, $\nu = 0.3$ and $\rho = 7800\,\mathrm{kg/m^3}$.

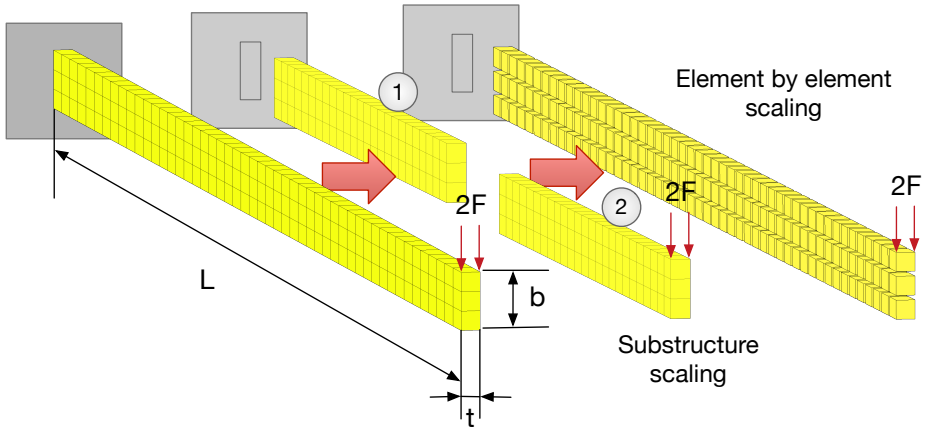


**FIGURE 8** Cantilever beam with tip load. Original geometry, dimensions and assembled global mesh (left), mesh partitioned into two subdomains for substructural (center) and mesh completely partitioned for element-by-element mass tailoring (right).

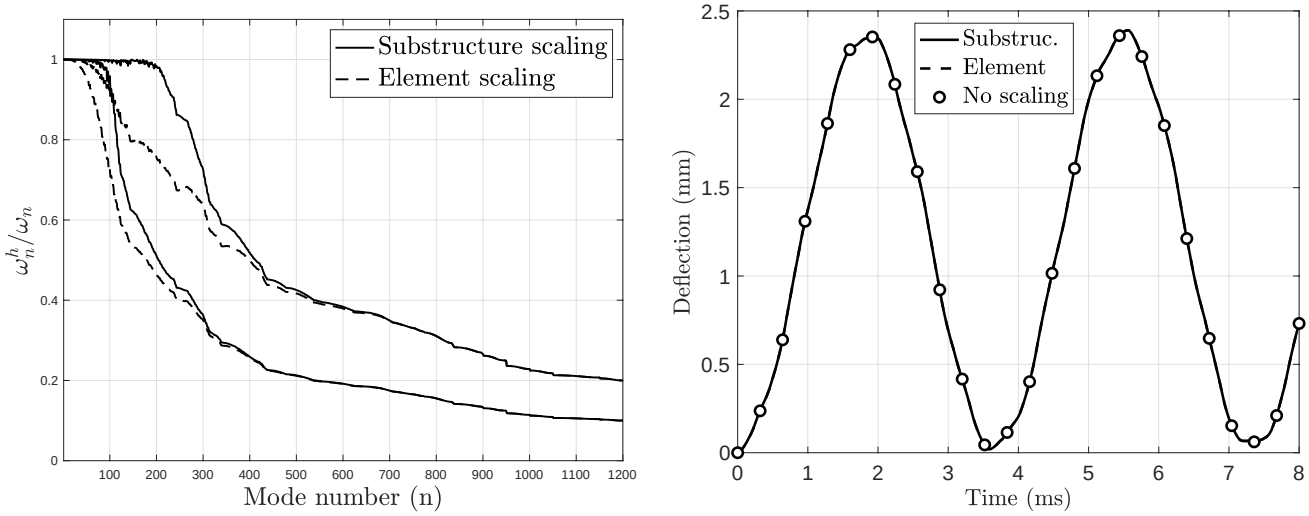


**FIGURE 9** Results of the tip loaded cantilever beam. Ratio of eigenfrequencies at two different levels of maximum frequency reduction $\mathsf{N}_{\mathsf{gain}} = \{5, 10\}$ using substructural and element-by-element mass tailoring (left). Beam deflection for maintained tip loads computed with stepsize gain factor $\mathsf{N}_{\mathsf{gain}} = 50$ (right).

The beam is discretized using a regular mesh of 150 hexahedrical elements and 408 nodes, with 50×3×1 divisions per side. One end of the beam is completely fixed and the other side has two vertical point loads of value $F = 1$ N. Two different cases are considered, first the tip load is fully applied at the first time step and maintained constant during the simulation. In the second case, the load is applied as two initial impulses 1 mm/s at the same points, in order to activate higher modes in the response of the beam.

In both cases, we perform a time-domain analysis integrating in time the response of the beam using the explicit central difference method (19). Initial conditions of the beam are assumed to be zero displacements and velocities, applying the tip load completely at the initial time-step.

Using element-by-element tailoring, for respective extensions of stepsize gain factors of $\mathsf{N}_{\mathsf{gain}} = 5$ and $\mathsf{N}_{\mathsf{gain}} = 50$, it is necessary to filter all the 18 higher modes of the element. Partitioning into two equal substructures of 75 hexahedrals and 208 nodes, on the contrary, produces 624 modes per subdomain, requiring a modification of 517 and 603 higher modes respectively for extensions $\mathsf{N}_{\mathsf{gain}} = 5$ and $\mathsf{N}_{\mathsf{gain}} = 50$ with substructure scaling.

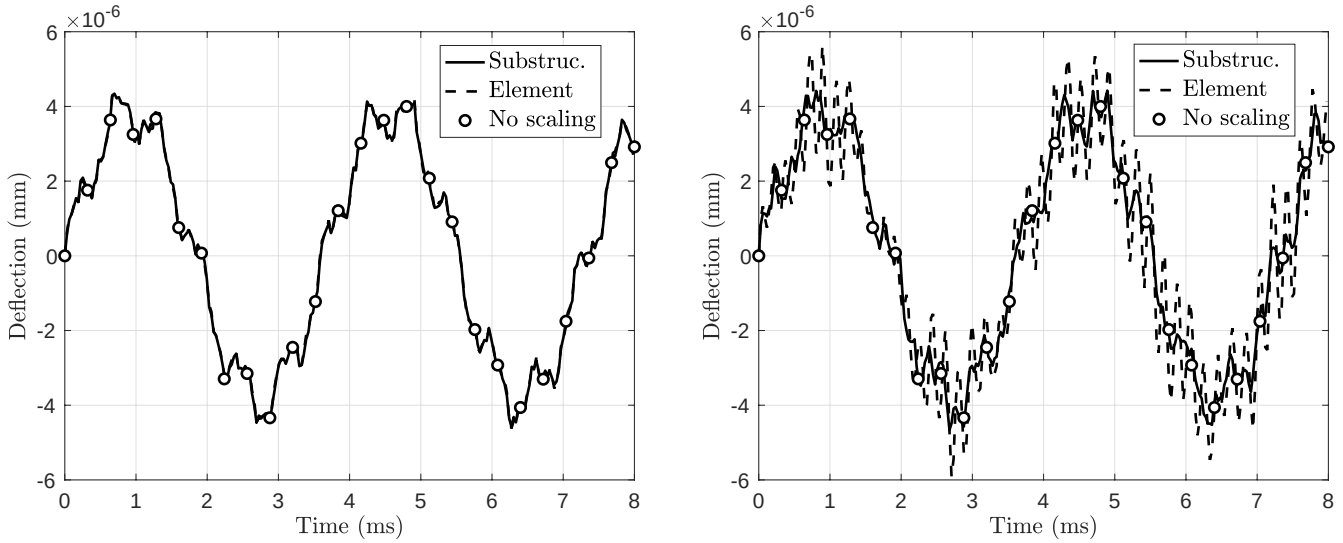


**FIGURE 10** Impulsive load on a cantilever beam. Tip deflection with different mass tailoring methods for reductions of the maximum frequency of stepsize gain factors $N_{gain} = 5$ (left) and $N_{gain} = 50$ (right). It is observed the effect of accuracy loss in the higher frequencies for the element-by-element tailoring.

We start analyzing the case of maintained tip loads. The results are shown in Figure 9 (right), where it is represented the evolution of the tip deflection of the beam obtained with both tailoring methods for a reduction of $N_{gain} = 50$. Classical selective mass scaling techniques applied to this problem[10] were capable of extending the critical time step with reasonable accuracy to a maximum of $N_{gain} = 10$ times. However, it should be noted that we are only exciting the lowest modes of the beam, where both methods show good accuracy.

Next, we study the case of two impulse loads where higher modes are excited. In Figure 10 it is represented the tip deflection for $N_{gain} = 5$ (left) and $N_{gain} = 50$ (right). It is clear that for moderate extensions of the critical time step, like $N_{gain} = 5$ in our example, both methods can provide enough accuracy. However, for lager time step extensions, $N_{gain} = 50$, element by element tailoring quickly starts loosing its accuracy, while substructural tailoring is able to maintain precision.

## 8 | DISCUSSIONS

Two mass matrix tailoring approaches, viz., the high-frequency filtering method (26) and the low-frequency preservation method (31), have been presented and their performance is assessed. We now offer the following observations:

- Both of the proposed methods preserve low-frequency eigenvectors and frequencies at or below the cut-off frequency.
- Regardless of the problem sizes and partitions numbers, the cut-off frequency is the upper bound frequency of the total system when the mass matrix is tailored by employing the proposed two methods.
- Efficiency of the proposed methods is facilitated by exploiting the low rank-update inversion formulas (28) and (35).
- The smaller the number of degrees of freedom per partition, the more efficient the resulting computational procedure. However, except for thin plates and shells (For example, in the case of thin plate models discussed in Section 7.3), elemental mass tailoring yields poorer accuracy than substructural partition procedures. We hope further studies would offer a sensible trades-off guide.

Finally, a word on applying the proposed large-step explicit integration is in order. In general, experience indicates that nonlinearities would bring about a minimum change in both higher frequencies and their mode shapes, whereas they can significantly change low frequency mode shapes. This suggests that for highly nonlinear problems, the high-frequency mode filtering method (26) is preferable, with a smaller number of elements per partition. This and more detailed explicit step marching procedures

(for example, partitioned solution of accelerations) are being actively investigated and we hope to report the outcome of the present ongoing studies in the near future.

## References


1. Courant R, Friedrichs K, Lewy H. On the partial difference equations of mathematical physics. *IBM Journal of Research and Development.* 1967;11(2):215–234.
2. Krenk S. Dispersion-corrected explicit integration of the wave equation. *Computer Methods in Applied Mechanics and Engineering*. 2001;191(8–10):975–987.
3. Gravouil A, Elguedj T, Maigre H. An explicit dynamics extended finite element method. Part 2: Element-by-element stable-explicit/explicit dynamic scheme. *Journal of Computational and Applied Mathematics.* 2009;198:2318–2328.
4. Idesman A, Schmidt M, Foley J. Accurate finite element modeling of linear elastodynamics problems with the reduced dispersion error. *Computational Mechanics.* 2011;47(5):555–572.
5. Park Kwang-Chun, Lim S. J., Huh H.. A method for computation of discontinuous wave propagation in heterogeneous solids: basic algorithm description and application to one-dimensional problems. *International Journal for Numerical Methods in Engineering*. 2012;91:622–643.
6. Cho S. S., Park Kwang-Chun, Huh H.. A method for multidimensional wave propagation analysis via component-wise partition of longitudinal and shear waves. *International Journal for Numerical Methods in Engineering.* 2013;95:212–237.
7. Hinton E, Rock T, Zienkiewicz O C. A note on mass lumping and related processes in the finite element method. *Earthquake Engineering & Structural Dynamics.* 1976;4(3):245–249.
8. Macek R W, Aubert B H. A mass penalty technique to control the critical time increment in explicit dynamic finite element analyses. *Earthquake Engineering & Structural Dynamics.* 1995;24(10):1315–1331.
9. Olovsson L, Unosson M, Simonsson K. Selective mass scaling for thin walled structures modeled with tri-linear solid elements. *Computational Mechanics.* 2004;34(2):134–136.
10. Olovsson Lars, Simonsson Kjell. Selective mass scaling for explicit finite element analyses. *International Journal for Numerical Methods in Engineering.* 2005;63(10):1436–1445.
11. Askes H, Nguyen D, Tyas A. Increasing the critical time step: micro-inertia, inertia penalties and mass scaling. *Computational Mechanics.* 2011;47(657–667).
12. Cocchetti Giuseppe, Pagani Mara, Perego Umberto. Selective mass scaling and critical time-step estimate for explicit dynamics analyses with solid-shell elements. *Computers & Structures.* 2013;127:39–52.
13. Tkachuk Anton, Bischoff Manfred. Variational methods for selective mass scaling. *Computational Mechanics.* 2013;52:563–570.
14. Lombardo M, Askes H. Lumped mass finite element implementation of continuum theories with micro-inertia. *International Journal for Numerical Methods in Engineering.* 2013;96(7):448–466.
15. Hetherington Jack, Askes Harm. A mass matrix formulation for cohesive surface elements. *Theoretical and Applied Fracture Mechanics.* 2014;69:110-117.
16. Tkachuk Anton, Bischoff Manfred. Local and global strategies for optimal selective mass scaling. *Computational Mechanics.* 2014;53:1197–1207.
17. Frias G, Aquino W, Pierson K, Heinstein M, Spencer B. A multiscale mass scaling approach for explicit time integration using proper orthogonal decomposition. *International Journal for Numerical Methods in Engineering.* 2014;97:799–818.

18. Belytschko T., Liu W.K., Moran B., Elkhodary K.. *Nonlinear Finite Elements for Continua and Structures*. John Wiley & Sons, Ltd.; 2nd ed.2014.

19. Tkachuk Anton, Bischoff Manfred. Direct and sparse construction of consistent inverse mass matrices: general variational formulation and application to selective mass scaling. *International Journal for Numerical Methods in Engineering.* 2015;101(6):435–469.

20. Hartmann Stefan, Benson David J. Mass scaling and stable time step estimates for isogeometric analysis. *International Journal for Numerical Methods in Engineering.* 2015;102(3–4):671–687.

21. Großeholz Georg, Soares Jr. Delfim, Estorff Otto. A stabilized central difference scheme for dynamic analysis. *International Journal for Numerical Methods in Engineering.* 2015;102(11):1750-1760.

22. Felippa Carlos A, Guo Qiong, Park Kwang-Chun. Mass Matrix Templates: General Description and 1D Examples. *Archives of Computational Methods in Engineering.* 2015;22(1):1–65.

23. González José A., Kolman R., Cho S. S., Felippa C. A., Park K. C.. Inverse Mass Matrix via the Method of Localized Lagrange Multipliers. *International Journal for Numerical Methods in Engineering.* 2017;113(2):277–295.

24. Park K. C., Felippa C. A.. A variational framework for solution method developments in structural mechanics. *Journal of Applied Mechanics.* 1998;65(1):242–249.

25. Park K. C., Felippa C. A.. A variational principle for the formulation of partitioned structural systems. *International Journal for Numerical Methods in Engineering.* 2000;47:395–418.

26. González José A., Kopačka J., Kolman R., Cho S. S., Park K. C.. Inverse mass matrix for isogeometric explicit transient analysis via the method of localized Lagrange multipliers. *International Journal for Numerical Methods in Engineering.* 2019;117:939–966.

27. González José A., Park K. C.. A simple explicit-implicit finite element tearing and interconnecting transient analysis algorithm. *International Journal for Numerical Methods in Engineering.* 2011;89(10):1203–1226.

28. Woodbury Max A.. *Inverting modified matrices.* : Memorandum Rept. 42, Statistical Research Group, Princeton University, Princeton, NJ, 4pp; 1950.

29. Irons B. M., Tregarne G.. A bound theorem in eigenvalues and its practical applications. In: :19-21Rep. No. AFFDL TR 71-160, Wright-Patterson Air Force Base, Ohio; 1971.

30. Fried I.. Bounds on the extremal eigenvalues of the finite element stiffness and mass matrices and their spectral condition number. *Journal of Sound and Vibration.* 1972;22(4):407-418.